
Journal of Intelligent and Robotic Systems **36:** 23–44, 2003.

Design and Calibration of an Opto-mechanical Appliance for 3D Non-contact Orthopedic Measurements

Part II: Calibration Methodology and Experimental Results

ROBERTO CARACCIOLO* and ALBERTO TREVISANI
Department of Management and Engineering (DTG), Università di Padova, 36100 Vicenza, Italy; e-mail: caracciolo@gest.unipd.it

(Received: 12 March 2001; in final form: 11 December 2001)

Abstract. A multistep iterative calibration methodology for the opto-mechanical system introduced in Part I is proposed. The methodology makes use of a monoview coplanar set of control points, whose number has been determined on the basis of both geometrical considerations and the results of a statistical analysis aiming at assessing the procedure stability in the case of noisy image data. The calibration procedure is carried out comparing the theoretical and observed images of the calibration pattern. Both synthetic and real data have been employed to test the calibration procedure, which proved to be accurate and efficient. The experimental results achieved by the calibrated system are satisfactory in terms of measurement precision.

Key words: 3D scanning, structured light vision, multistep iterative calibration.

1. Introduction

An opto-mechanical system for 3D non-contact measurements has been presented in Part I of this work. The system has been conceived and developed to perform accurate, reproducible, fast and non-invasive measurements of human foot shapes and to reconstruct 3D foot models. It has been explained how the system operates: the foot surface is scanned by means of a moving CCD camera which can sense the lines of light projected on the foot surface by two lasers moving together with the camera like a rigid body. The two lasers are used in sequence to prevent shadowing. Images are captured at known positions on a circular trajectory and then aggregated to generate a 3D model of the foot. The model of the foot can be processed to infer geometrical information, and compared to a selected standard shoelast in order to design a customized shoelast.

In the description of the system operating method, it has been underlined that all the lines of light sensed by the camera lie on the plane surface generated by the working laser. A biunique correspondence has therefore been established between the set of points on the light plane within the field of view of the camera and the

* Corresponding Author.

set of points on the image plane. The transformation between the 2D image plane reference and the 2D computer image reference has allowed defining the mapping from the light plane coordinates to the computer image coordinates. Finally, given the geometry of the system, because an encoder directly provides the position of the laser plane in the 3D world reference, it has been possible to estimate the coordinates of one point in the 3D world reference from its image in the frame memory. Hence a complete kinematic and optical model of the system has been developed, accounting for the main internal parameters of the camera.

To speed up data acquisition an appropriate data structure and acquisition procedure have been introduced. Through the mathematical model of the system one calibration table for each laser is created. The elements of such tables are the coordinates in the light plane reference of the projections of all the pixels on the two light planes. Each calibration table therefore associates the computer image coordinates of all the pixels, to the light plane coordinates of the corresponding points on a light plane. While scanning, the use the tables allows determining immediately the coordinates on the light plane reference of the points sensed by the camera. The 3D position of the points sensed can be subsequently computed combining these pieces of information with the angular position of the light plane. The use of such a two step acquisition procedure, in spite of employing the mathematical model of the system straight, makes the acquisition process faster.

Both the steps of the acquisition procedure lead to correct results only if the overall opto-mechanical system is carefully calibrated. Defining a procedure which enables an accurate evaluation of the optical and geometrical parameters of the system mathematical model is therefore a crucial aspect of the system design, because it affects the accuracy and the reproducibility of the measurements that can be executed.

A simultaneous calibration of the mechanical and optical components of the system is required: not only are the camera intrinsic (internal geometrical and optical characteristics of the camera) and extrinsic (expressing the 3D position and orientation of the camera) parameters to be determined, but also the relative positions between either lasers and the camera. The problem of calibrating the system is therefore different from that of calibrating just a camera and involves considering the mathematical model of the global system.

Several camera calibration techniques have been proposed by the photogrammetry and the computer vision communities. Comprehensive reviews of the state of the art in this area have been presented by Tsai (1987) and more recently by Batista et al. (1999). The main differences among the techniques classified by these authors are in the use of a linear or nonlinear camera model and computation procedure, in the number of unknowns of the model, in the choice of the calibration pattern, in the use of a camera executing accurate and controlled movements, and in the capability of calibrating with or without determining the camera physical parameters (which is called, respectively, explicit and implicit calibration).

Tsai (1987) has also introduced a well known two-step calibration method: a radial alignment constraint (RAC) is used to derive a closed-form solution for most of the calibration parameters, then an iterative scheme is used to determine the value of the other parameters. From the computational viewpoint this method is very efficient because only a relatively small number of parameters is estimated in the iterative step. In the work by Lenz and Tsai (1988), the same technique has been extended to include two additional intrinsic parameters: the horizontal scale factor and the image center. There values are determined iteratively in the second step of the method. Another important example of two-step approach has been proposed by Weng et al. (1992). A major difference between these techniques and the one by Tsai is that not a few, but all the parameter estimates are iteratively improved in the second step, which consist of a nonlinear optimization based on a camera model incorporating, as initial guesses, the solutions obtained using the noniterative algorithm of the first step.

Among the intrinsic parameters included in the researchers' camera models, lens distortion has a critical importance. Ignoring lens distortion entails solving linear equations only, which speeds up the calibration process, but has the major drawback that considerably less precise results are generally obtained. In the aforementioned work by Tsai (1987) radial geometric distortion has been included for the first time, while Weng et al. (1992) proposed a more accurate model of lens distortion, including both radial and tangential distortion. More recently Wei and De Ma (1994), and Batista et al. (1999) have proposed calibration methodologies which can model lens distortion still using linear computation. The work by Wei and De Ma (1994) represents an extension of the original two-plane method, introduced by Martins et al. (1981), and is an example of implicit camera calibration: the camera is calibrated without computing its physical parameters, but considering some intermediate parameters to which no physical meaning is attached. Batista et al. (1999) presented an iterative, multistep methodology requiring only linear computations. Because monoplane calibration points are employed, this technique requires a first-guess solution for the intrinsic parameters. During the iterative procedure the accuracy of the intrinsic parameter estimates is progressively increased.

Most of the available calibration techniques require the use of specifically designed calibration patterns: Tsai (1987) used a sixty-control-point pattern to carry out the calibration procedure while Zhuang and Wu (1996), who proposed a technique based on Tsai's method but suitable for the near-parallel calibration pattern configuration, employed a pattern with 10×10 dot array points. Some authors have proposed the use of planar geometric object calibration patterns: in (Wang and Tsai, 1991) the geometric information on the vanishing line associated to the vanishing points of the parallel sides of an hexagon is used to infer the camera orientation and the focal length. Basu and Ravi (1995), and Yang and Hu (1998) have recently suggested calibrating camera intrinsic parameters without using special patterns for calibration but controlling the camera to perform

some specially designed motions. These techniques are called 'active calibration' or 'self-calibration': the camera is required to be able to perform accurate and controlled movements.

Camera calibration methodologies are rarely performed making use of a single picture of a planar calibration pattern. Admittedly, as it has been underlined by Batista et al. (1999), performing a global camera calibration using, for example, a monoview coplanar set of points is impossible due to the singularity obtained with the calibration equations. To overcome such a difficulty, two main approaches have been considered in literature:

- moving the camera so as to perform an active calibration, which indirectly leads to a multiplane calibration;
- performing a partial calibration, in which some of the parameters are considered known.

In this paper the second of the aforementioned approaches is followed to calibrate the system making use of a monoview coplanar set of points. Some intrinsic parameters of the camera are therefore assumed to be known in advance while the intrinsic parameters most affecting the accuracy in the system measurement have been included among the parameters calibrated.

The calibration of the system is performed through a four-step procedure whose core is based on the comparison between some selected geometrical features of the observed image of the calibration pattern and the same features of the expected, or theoretical, image of the pattern. The theoretical positions of the control points are computed making use of a mathematical model derived from the one described in Part I. The four steps constituting the procedure are repeated iteratively until a satisfactory similarity between the theoretical and observed images of the calibration pattern is attained.

Two calibration tables represent the fundamental output of the calibration procedure. The two tables are generated introducing into the system model the values of the geometrical and optical parameters estimated through the calibration procedure, and computing, for each pixel, the coordinates of its projection on the laser plane.

The number of control points comprising the calibration pattern has been determined on the basis of some geometrical considerations and the results of an extensive statistical analysis aiming at assessing the calibration procedure stability in regard to image acquisition noise, and how such stability is influenced by the number of control points. The effect of the noise in image data has been simulated adding normally distributed random error to the control point positions.

The calibration procedure has been tested with both real and synthetic data. Simulations have allowed an accurate tuning of the procedure. The experimental results obtained calibrating the laboratory prototype are characterized by a very good value of the index introduced to evaluate the calibration performance. Finally, the accuracy and resolution in the measurements made by the calibrated system are reported.

2. Multistep Calibration

The need to obtain accurate measurements from the proposed opto-mechanical system has suggested developing a calibration procedure taking into consideration the global system including the lasers. The calibration technique proposed is performed by means of a monoview coplanar set of points, called control points. The objective is evaluating the deviation from the nominal values of the geometrical and optical parameters of the system by analyzing the discrepancies between the observed positions of the control point images and the theoretical positions the same images would occupy if the nominal values of the parameters were respected. The observed positions are those of the control points belonging either to the real (acquired) image of the calibration pattern, or to the distortion-free image computed from the one acquired compensating the effect of radial distortion and image data noise. The theoretical, or expected, image projections of the control points are computed by means of the mathematical model of the system, and with reference to either the nominal or the most recently determined values of the geometrical and optical parameters.

2.1. CALIBRATION PATTERN

The planar calibration pattern employed is composed of a sheet of paper on which a set of black circles is drawn by a laser printer. The sheet of paper is white, rectangular (21 $\times$ 29.7 cm) and of negligible thickness. The circles are arranged in rows and columns which are at known distances from one another and from the center of the calibration pattern represented by the intersection point of two very thin and continuous orthogonal lines. The most appropriate number of circles of the pattern has been determined according to the statistical considerations reported in Section 3.

To simplify the calibration procedure the calibration sheet is laid on the machine steady footboard. Only if the sheet is accurately positioned on the footboard is it possible to reconstruct the expected computer image of the calibration pattern by means of the mathematical model of the system. A correct positioning of the calibration pattern has been assured by the aforementioned thin lines printed on it:

- one of the lines is aligned with the projection of one light plane on the footboard,
- the intersection of the two lines is made to coincide with the intersection of the two light plane projections, which coincide with the center of rotation of the laser-camera system.

Since the relative angle of the two lasers is known in advance (they form a precise angle of 90°), it is not important which light plane is chosen to accurately position the calibration sheet: the geometrical information gathered at the end of the calibration procedure can be easily transferred to the other laser. When the sheet is correctly positioned, and the nominal values of the geometrical and optical parameters of the system are respected, the centroid of one circle (‘central point’)

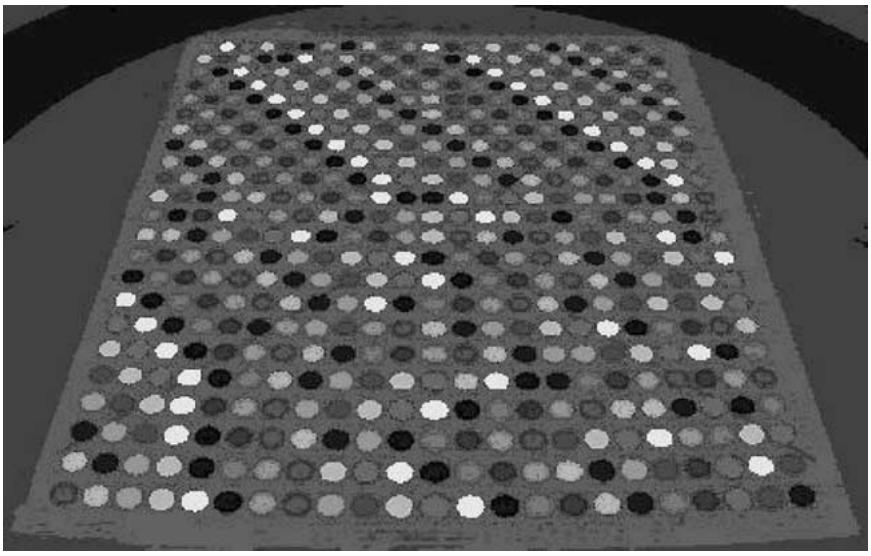

Figure 14. Processed image of the calibration pattern highlighting the circles, considered independent objects.

coincide with the intersection of the camera optical axis and the footboard plane. As it is shown below, such a geometrical device has been introduced to simplify the comparison between the expected and real images of the circles.

The centroids (i.e. the centers of area) of the ellipses, projections of the circles on the image plane, are the control points used for calibration. The observed positions of the centroids in the computer image reference have been determined by means of the image processing toolbox *Evision 5.1* developed by *Euresys*. Figure 14 shows an image of the calibration sheet, lying on the prototype footboard, as it is viewed and captured by the camera. The image has been processed through the aforementioned toolbox so as to get the centroids of the circles. Each originally black circle detected, is considered a different object and is displayed in a different color (gray scale).

The theoretical positions of the coplanar control points are computed starting from the nominal geometry of the calibration pattern and making use of a kinematic and optical model of the system derived from the one described in Part I. The chief changes that need to be introduced in the model are driven by the fact that the control points do not lie on the light plane but on the plane of the system steady footboard. The mathematical model of the system is therefore to be modified so as to allow computing the position, in the camera reference, of any point lying on the footboard plane starting from its computer image coordinates.

Following the same approach as in Part I, matrices **H** and **K** must take the form:

$$\mathbf{H} = \begin{bmatrix} -y_I & -f & 0 \\ -z_I & 0 & -f \\ E & F & G \end{bmatrix}, \tag{23}$$

$$\mathbf{K} = \begin{bmatrix} -y_I f \\ -z_I f \\ -I \end{bmatrix} \tag{24}$$

where E, F, G and I are the coefficients of the equation of the footboard plane on the camera coordinate system. The explicit expressions of E, F, G and I and how they may be obtained are reported in the Appendix.

The different values in the third row of the matrices **H** and **K** represent the only differences between the model used to calibrate the system and the model used to acquire and process data. Therefore the geometrical and optical model employed at this stage of the work derives from the one presented in Part I just substituting Equations (23) and (24) for Equations (8) and (9).

2.2. PARAMETERS CALIBRATED

In this paper the parameters which allow determining the position and orientation of the camera relative to the laser plane considered are called extrinsic parameters, while those expressing the internal geometrical and optical characteristics of the camera are called intrinsic parameters.

The following extrinsic parameters are calibrated in the implemented multistep calibration procedure:

- (t_x, t_y, t_z): the coordinates of the origin of the world coordinate system in the camera coordinate system;
- α: the angle made by the projection of the light plane and of the axis X_C on the footboard plane;
- φ: the inclination of the axis X_C with respect to the footboard plane;
- σ: the rotation of the camera about the axis X_C.

The mentioned angles are shown in Figures 5(a), (b), and (c) of Part I.

The camera intrinsic parameters calibrated are:

- K_1 and K_2: the coefficients of radial distortion;
- f: the effective focal length of the camera.

These are the intrinsic parameters whose influence on the acquired image proved to be relevant. Some other intrinsic parameters of the camera, such as the computer image coordinates of the optical principal point (C_y, C_z) and the horizontal scale factor s_y, are not calibrated. They are assumed to be known in advance and might be estimated by means of a precalibration procedure. It has been assumed that the coordinates (C_y, C_z) correspond to the center of the image frame buffer, and that s_y is equal to 1.025.

2.3. CALIBRATION PROCEDURE

A four-step approach is adopted to calibrate the system. The four steps must be executed in the unalterable sequence in which they are described below.

First of all, a nonlinear optimal estimation process is carried out to calibrate the two coefficients of radial distortion K_1 and K_2. The positions of the observed images of the control points are re-computed so as to obtain a distortion-free image of the calibration pattern, compensating the effect of lens distortion.

A further re-computation of the coordinates of the control point images is executed at the second step: because the control points in the calibration pattern are sorted out in rows and columns, the misalignment of the images of the points can be traced back mainly to image acquisition noise. A significant reduction of the effect of acquisition noise has been obtained re-computing the coordinates of the control point images so as to reduce the point misalignment: for each row and column of control point images the fitting straight lines have been determined by least square method. The intersection points among all the fitting lines have then been considered the actual control point images. Through this geometrical device, not only can the effect of image acquisition noise be considerably reduced, but also the position of the control points can be determined with subpixel accuracy.

In the third step of the calibration procedure, an iterative process is carried out to compute accurate initial estimates of the extrinsic parameters of the system, starting from appropriate initial guesses which are the nominal values of the parameters. The parameter estimates are calculated through the comparison between some geometrical features of the observed image of the calibration pattern and the same features of the expected image.

The estimates obtained in the third step are subsequently used in the last step of the procedure, which consists of a nonlinear iterative optimization process yielding the improved estimates of the extrinsic parameters and the effective focal length of the camera.

In summary the suggested calibration procedure comprises the following steps:

1. calibration of the two coefficients of radial distortion and re-computation of the positions of the real images of the control points to get a distortion-free image;
2. reduction of the acquisition noise in the distortion-free image data;
3. iterative computation of the initial estimates of the extrinsic parameters of the system starting from the nominal values;
4. nonlinear iterative calibration of the extrinsic parameters and of the camera focal length.

The third and fourth steps, described below in detail, represent the core of the implemented methodology.

In the third step of the procedure, the extrinsic parameter estimates are computed in an unalterable sequence which has been established studying the effect of the variation of the value of each extrinsic parameter on the positions of the control point images. Figures 15 through 20 schematically reproduce the effect for each parameter calibrated, a twelve-circle calibration pattern is considered for clarity. The figures have been obtained adding a large constant value to the nominal value of one parameter at a time, and plotting the theoretical control point projections on

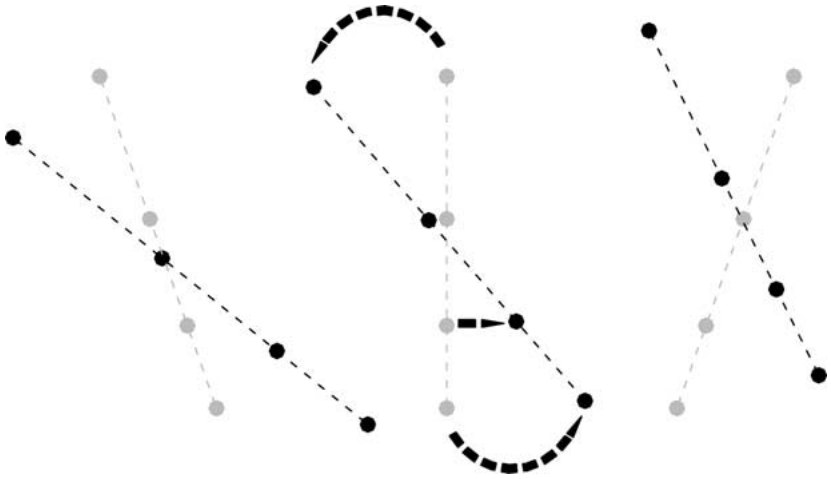

Figure 15. Schematic representation of the effect on the control point images of a variation of α.

the image plane when no variations of the parameters are introduced (gray circles) and after the parameter alteration (black circles). The arrows underline the chief changes in the image geometry and position.

With reference to each extrinsic parameter, the comparison between the values assumed, in the distortion-free and theoretical images of the calibration pattern, by the geometrical feature which is most affected by the parameter variation is employed to yield the parameter estimate. Besides, because only approximate relations are established among the geometrical features variations and the deviations from the nominal values of the parameters, iterative processes are necessary to compute the estimates of the parameters accurately. The mathematical model of the system is iteratively updated with a new value whenever a better estimate of a parameter is found. Hence, the theoretical image of the control points is recomputed, taking into account the error identified: the more accurate the estimates of the parameters are, the better the theoretical and distortion-free images overlap. This step of the calibration procedure ends when the geometrical differences between the two aforementioned images are negligible.

The third step calibration sequence starts computing the value of the three parameters α, σ, and t_y, whose value variations cause effects, on the geometry of the pattern image, which can be effectively decoupled. It can be observed in Figure 15 that a variation (Δ) of the value of the angle α makes the slope of the rows and columns of the calibration pattern change. In particular the variation of the slope of the columns is more accentuated than that of the rows, which has suggested computing the value of α through the equation:

$$\Delta\alpha = K_\alpha \sum_{i=1}^{M} (n_i^* - n_i) \tag{25}$$

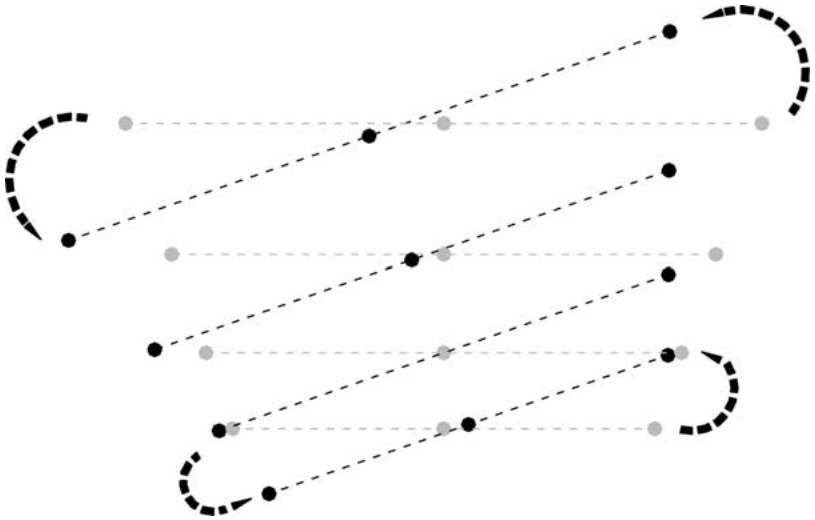

Figure 16. Schematic representation of the effect on the control point images of a variation of σ.

where:

- M is the number of columns of control points,
- n_i and n_i^* are the slopes of the ith columns of the theoretical and distortion-free images,
- K_α is the gain.

A similar effect is generated by a variation of the angle σ (Figure 16), which, unlike a $\Delta\alpha$, makes the pattern image rotate as a rigid body about the central point. The row slopes are not changed by any other parameter variations, therefore it is possible to compute σ immediately after α, by means of the following equation:

$$\Delta\sigma = K_\sigma \sum_{i=1}^{N} (m_i^* - m_i) \tag{26}$$

where:

- N is the number of rows of the calibration pattern,
- m_i and m_i^* are the slopes of the ith rows of the theoretical and distortion-free images,
- K_σ is the gain.

The third parameter considered is t_y, whose variation just causes an horizontal translation of the image (Δy_c in Figure 17). Apart from α, t_y is the only parameter causing this effect. In order to speed up the calibration procedure it has been decided to focus only on the points of the central column, which does not affect the estimate correctness since all the control points belonging to the same row undergoes the same translation. Additionally, because the pattern image is generally tilted with respect to the image plane coordinate system, the translation

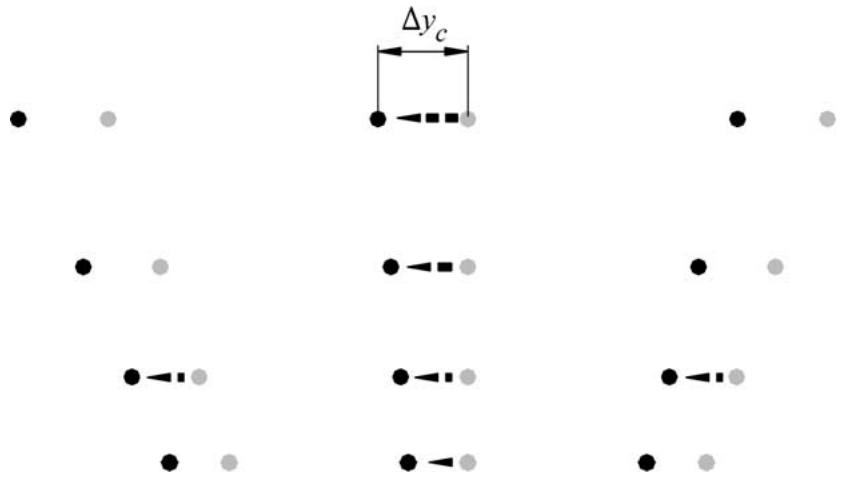

Figure 17. Schematic representation of the effect on the control point images of a variation of t_y.

to be considered is not along the axis Y_I but along the row passing through the central point in the distortion-free image. The equation employed is the following:

$$\Delta t_y = K_y \sum_{i=1}^{N} \left[(y^*_{i,\mathrm{c}} - y_{i,\mathrm{c}}) \cdot \cos(\zeta^*_{\mathrm{c}}) + (z^*_{i,\mathrm{c}} - z_{i,\mathrm{c}}) \cdot \sin(\zeta^*_{\mathrm{c}}) \right] \tag{27}$$

where N has the same meaning as in Equation (26) and:

- $y_{i,\mathrm{c}}$ and $z_{i,\mathrm{c}}$ are the coordinates, in the computer image reference, of the control points belonging to the central column and the ith row of the theoretical image,
- $y^*_{i,\mathrm{c}}$ and $z^*_{i,\mathrm{c}}$ are the coordinates, in the computer image reference, of the control points belonging to the central column and the ith row of the distortion-free image,
- ζ^*_{c} is the slope angle of the row passing through the central point in the distortion-free image,
- K_y is the gain.

As shown in Figures 18–20, variations of the parameters t_z, φ, and t_x do not produce decoupled effects on the calibration pattern image geometry. Very similar effects are generated. In particular, all the variations cause vertical displacements of the control points belonging to the central column. The comparison among the aforementioned figures reveals that only a variation of t_z does not cause changes of the relative distances among the points on the same row, while only when a variation of t_x is introduced, the central point does not move and a radial shifting of all the other points occurs, generating a uniform magnification of the image. This effect allows computing t_x separately, once the values of the parameters t_z and φ have been determined.

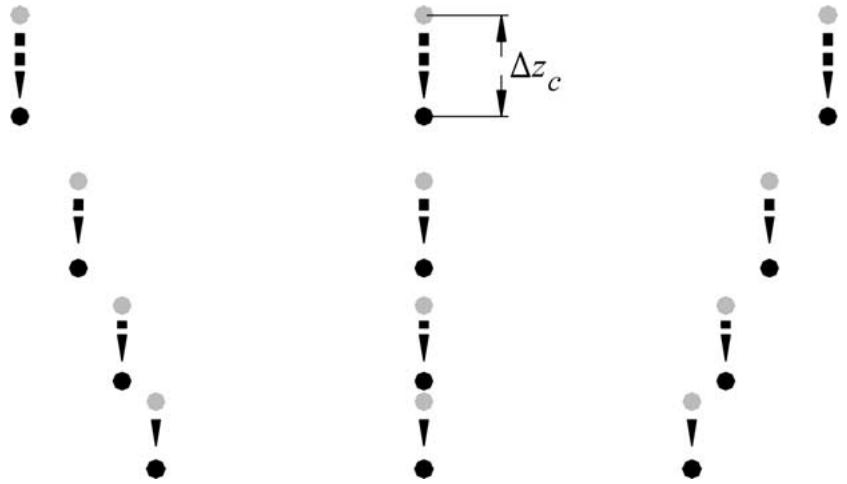

Figure 18. Schematic representation of the effect on the control point images of a variation of t_z.

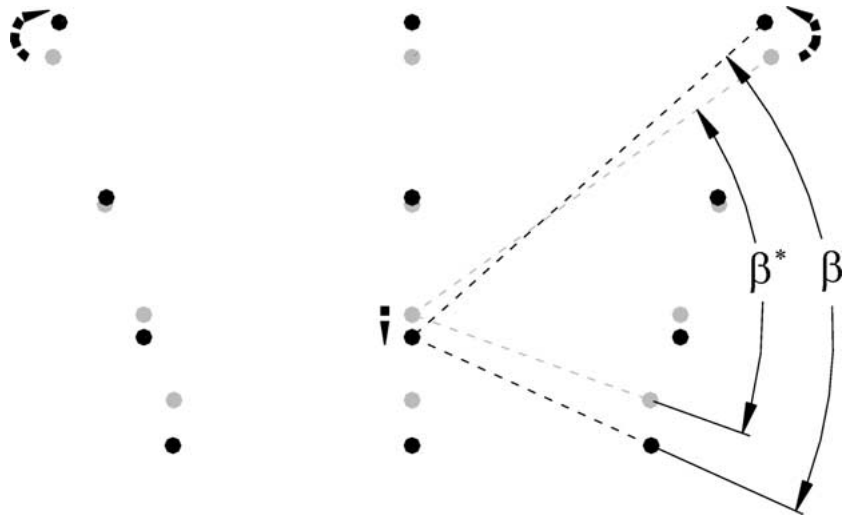

Figure 19. Schematic representation of the effect on the control point images of a variation of φ.

The very similar effects produced, make it impossible to study t_z and φ separately. Their values are estimated through a single iterative process based on the analysis of the vertical translations of the points in the central column and the variation of the angles β_i and β_i^* (see Figure 19). Because of the mutual influence between t_z and φ, each time a new estimate of either t_z or φ is computed, and the model of the system is updated, the change affects also the geometrical feature associated with the other parameter, which consequently needs to be recomputed. This process is carried out until the reciprocal effects are negligible.

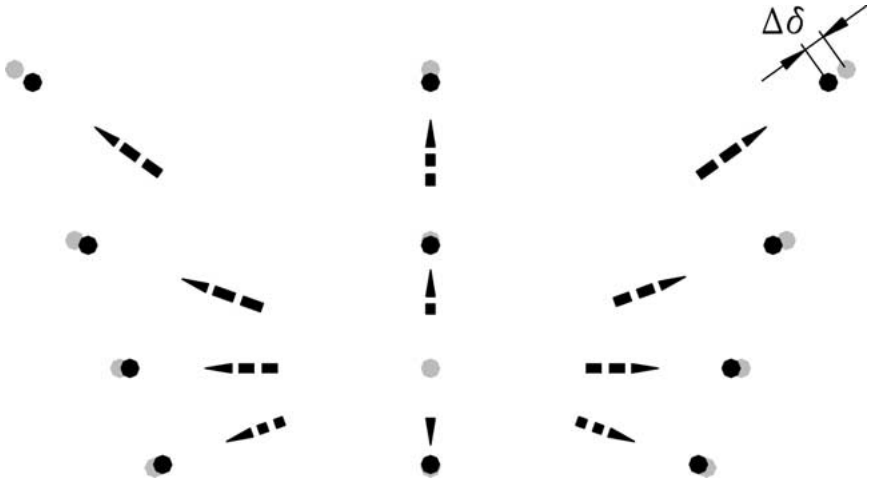

Figure 20. Schematic representation of the effect on the control point images of a variation of t_x.

The two equations employed iteratively are:

$$\Delta t_z = K_z \sum_{i=1}^{N} \left[(y^*_{i,c} - y_{i,c}) \cdot \sin(\zeta^*_c) + (z^*_{i,c} - z_{i,c}) \cdot \cos(\zeta^*_c) \right], \tag{28}$$

$$\Delta\varphi = K_\varphi \sum_{i=1}^{N/2} (\beta^*_i - \beta_i) \tag{29}$$

where:

- $y_{i,c}$, $z_{i,c}$, $y^*_{i,c}$, $z^*_{i,c}$, ζ^*_c, and N have the same meaning as in Equation (27),
- β_i and β^*_i are the angles formed, respectively in the theoretical and distortion-free calibration pattern images, by the lines connecting the central point to the last point of the ith row and to the last point of the $(N - i + 1)$th row. To get better estimates, the values of these angles and of those obtained considering the first point of each row in place of the last point have been used to get mean values.
- K_z and K_φ are the gains.

As previously explained, the last extrinsic parameter to be computed during the third step of the calibration procedure is t_x. A variation of this parameter causes a uniform magnification of the calibration pattern image, the center being the central point (Figure 20). A good estimate of the magnification factor and therefore of Δt_x is the variation of the distance between the image of the central point and the image of the points in the boundary of the calibration pattern:

$$\Delta t_x = K_x \sum_{i=1}^{C} [\delta^*_i - \delta_i] \tag{30}$$

where:

- C is the total number of points in the boundary of the calibration pattern;
- δ_i indicates the distance between the ith point in the boundary and the central point, measured in the theoretical image;
- δ_i^* indicates the distance between the ith point in the boundary and the central point measured in the distortion-free image of the calibration pattern;
- K_x is the gain.

An improvement in the accuracy of the estimate of the extrinsic parameter values is achieved in the fourth step of the calibration procedure through an unconstrained nonlinear optimization process. The optimization process aims not only at further increasing the precision of the initial estimates yielded by the third step but also at calibrating the effective focal length of the camera, considering the value supplied by the manufacturer an appropriate initial guess. The algorithm used in the iterative procedure is the Nelder–Mead simplex search implemented in the function 'fmins' of the language *Matlab* by *The Mathworks Inc*. The iterative process terminates when the local minimum of an objective function of the six extrinsic parameters and the focal length is found. The objective function chosen is the standard deviation (SD) of the distance, measured in the computer image reference, between corresponding points in the distortion-free and expected images of the calibration pattern. The value assumed by the standard deviation is an index of the accuracy of the output of the calibration process, since the lower the standard deviation, the higher the precision reached by the procedure. Theoretically the mean of the distance between corresponding points should be zero, which leads to the following formula for the standard deviation:

$$\mathrm{SD} = \sqrt{\frac{\sum_{i=1}^{R} [(y_i - y_i^*)^2 + (z_i - z_i^*)^2]}{R}} \tag{31}$$

where:

- y_i and z_i are the coordinates, in the computer image reference, of the expected image of the ith control point;
- y_i^* and z_i^* are the coordinates, in the computer image reference, of the distortion-free image of the ith control point;
- R is the number of control points.

The coordinates y_i and z_i are functions of the six extrinsic parameters and the focal length because they are computed by means of the mathematical model of the system. With reference to the other intrinsic parameters, the two coefficients of radial distortion have already been calibrated, and both the coordinates of the optical principal point and the horizontal scale factor are assumed to be known in advance (see Section 2.2).

3. Statistical Results Affecting the Calibration Pattern Design

The performance of the implemented calibration methodology largely depends on the accuracy with which the positions of the image plane projections of the circles drawn on the calibration pattern are measured through the camera. Image acquisition noise, which is caused by image digitization and by the specific technical features of the CCD sensor, affects the accuracy in measurements. As it is mentioned in the previous section, the second step of the calibration procedure has been introduced to reduce the effect of image acquisition noise. For each row and column of control points the fitting straight lines are used to re-compute the point positions. Therefore, the higher the number of control points on the rows and columns, the more the coordinates of the intersection points of the fitting lines provide precise estimates of the control point coordinates, and consequently, the less affected the system is by acquisition noise. On the other hand, the finite size of the calibration pattern represents a constraint to the maximum number of circles that can be drawn. In fact, increasing the number of circles implies drawing smaller and closer circles, which can be hardly recognized and separated by the camera. The choice of the most appropriate number of control points has been made on the basis of the results of a statistical analysis accomplished to verify the calibration procedure stability in regard to image acquisition noise, and how the stability is influenced by the number of control points. The pattern chosen on the basis of such analysis possesses a number of control points sufficient to reduce the influence of acquisition noise effectively.

Acquisition noise can be well represented by a stochastic variable and has therefore been simulated adding random error to the coordinates of the control points in the image plane reference. The random error introduced is normally distributed with mean zero and 2σ (σ = standard deviation) corresponding to a centroid displacement of 1.6 mm measured on the plane of the calibration pattern. This value represents half the maximum dimension of a pixel projection on the calibration plane, and can therefore be considered a large error in the estimate of the position of the centroid of the circles. After simulating the effect of acquisition noise, the calibration procedure is carried out to evaluate its stability to the noise. The first step is not executed because the effect of radial distortion is not simulated in the statistical analysis, which focuses on the third step of the calibration procedure: the one most affecting the final result. Therefore only the extrinsic parameters $t_x, t_y, t_z, \alpha, \varphi$, and σ are taken into consideration. The statistical analysis comprises five phases each leading to an intermediate result, the final result is inferred combining such results.

In the third step of the calibration procedure the error made on the estimate of each extrinsic parameter is computed comparing a specific geometrical feature of the distortion-free image of the calibration pattern with the same feature of the theoretical image. The objective of the first phase of the statistical analysis is investigating the influence of acquisition noise on the value of these geometrical

features, which are those already considered in the third step of the calibration procedure described in the previous section. To evaluate such influence, a known quantity is added to the nominal value of one extrinsic parameter at a time. This quantity modifies the value of the geometrical feature associated to the parameter. Random error is than added to the control point coordinates in order to simulate the effect of acquisition noise, and the value of the geometrical feature is re-computed. The deviation between the value computed and the value initially imposed provides a good estimate of the influence of acquisition noise. All the geometrical features are studied separately.

Variations of 1 mm are introduced in the values of the parameters t_x, t_y, and t_z, while variations of 0.1° deg are introduced in the angles α, φ, and σ. Such values represent reasonable tolerance limits of the prototype and should therefore cause the maximum possible variations of the geometrical features considered. When studying each geometrical feature, two hundred and fifty simulations are executed. The high number of simulations guarantees that a representative number of random conditions is considered. The results of the simulations are then aggregated and summarized in an index called mean absolute relative deviation (m.a.r.d.), which is expressed as a percentage:

$$\text{m.a.r.d.} = \frac{1}{S}\left|\frac{\sum_{i=1}^{S}(\xi_i^* - \xi)}{\xi}\right| \cdot 100. \tag{32}$$

The terms of the m.a.r.d. have the following meaning:

- S is the number of simulations carried out (250),
- ξ is the value assumed by the geometrical feature considered when no random errors are added,
- ξ_i^* is the value assumed by the geometrical feature considered at the ith simulation.

Table II synthetically summarizes the results of this step of the analysis: it shows the value assumed by the m.a.r.d. when acquisition noise is simulated and the aforementioned variations are added to the values of parameter written in the first row. For brevity, the results concerning only four different calibration patterns are considered in the table, the number of their rows and columns of circles are reported in the first column. The output data shows a predictable result: a marked reduction

Table II. Value of the m.a.r.d. computed for each extrinsic parameter. The first column contains the number of rows and columns of control points of the calibration pattern considered

	t_x	t_y	t_z	α	φ	σ
5*5	0.082	16.6	0.789	0.142	0.135	21.2
15*15	0.035	10.0	0.070	0.042	0.057	6.8
21*21	0.026	8.1	0.037	0.029	0.052	4.6
51*51	0.015	5.0	0.018	0.011	0.029	1.8

of the m.a.r.d. takes place when the number of control points is increased. From this first phase of the analysis it results that the geometrical feature values which are more affected by acquisition noise are those associated with the parameters t_y and σ.

The second phase of the analysis investigates the relation existing between a per cent variation of each geometrical feature and the corresponding per cent error made on the estimate of the variation from the nominal value of each extrinsic parameter value. Establishing such relation allows employing the results of the previous phase to identify the influence of acquisition noise on the computed estimates of the parameter variations.

The effect of a 1%-variation of every geometrical feature on the estimated variation of the associated parameter is evaluated at this phase. No random error is introduced and again, the variations associated to the extrinsic parameters are 1 mm in t_x, t_y, and t_z, and 0.1° deg in α, φ, and σ. The absolute errors computed are reported in Table III. It can be noticed that the parameters t_x and φ exhibit a substantial sensitivity to a 1%-variation of the corresponding geometrical feature, while t_y and σ are only moderately affected. On the other hand, Table II shows that acquisition noise causes small per cent variations of geometrical features associated with t_x and φ, and ample variations of those associated with t_y and σ. Therefore, only combining the results of the first two phases can the influence of acquisition noise be assessed precisely.

In the third phase of the analysis the per cent errors on the estimates of the extrinsic parameters variations caused by acquisition noise are computed multiplying the results of the first and second phase. The values obtained are shown in Table IV.

Table III. Absolute per cent error on the estimate of the variation of each extrinsic parameter caused by a 1%-variation of the value of the corresponding geometrical feature

	t_x	t_y	t_z	α	φ	σ
5*5	563.0	1.0	3.2	395.1	275.1	1.0
15*15	518.0	1.0	13.1	402.7	278.2	1.0
21*21	509.0	1.0	16.1	405.2	276.1	1.0
51*51	496.3	1.0	18.0	408.7	277.3	1.0

Table IV. Per cent error on the estimates of the extrinsic parameters variations caused by acquisition noise

	t_x	t_y	t_z	α	φ	σ
5*5	46.2	16.6	2.5	56.1	37.1	21.2
15*15	18.1	10.0	0.9	16.9	15.9	6.8
21*21	13.2	8.1	0.6	11.7	14.4	4.6
51*51	7.4	5.0	0.3	4.5	8.0	1.8

Table V. Standard deviation caused by a 1%-error of the computed values of the extrinsic parameter variations (μm)

	t_x	t_y	t_z	α	φ	σ
5*5	0.0211	0.147	0.147	0.0261	0.0207	0.0229
15*15	0.0274	0.154	0.154	0.0279	0.0240	0.0244
21*21	0.0291	0.156	0.156	0.0275	0.0249	0.0239
51*51	0.0315	0.158	0.158	0.0293	0.0263	0.0255

Such a procedure leads to correct results only if the system behaves like a linear system. A comparison between the results attained multiplying the intermediate results of phase one and two, and those obtained computing directly the error on the extrinsic parameter variation estimates caused by acquisition noise, has empirically proved that, under the conditions studied, the linearization of the system does not introduce considerable errors: the absolute per cent error on the values computed considering the system linear ranges from 0.10% to 1.35%.

The results obtained at the end of the third phase allow estimating the average per cent error that may affect the estimate concerning each calibrated parameter. Yet, such information by itself does not allow drawing conclusions about the influence of acquisition noise on the achievable accuracy of the calibration procedure and about the most appropriate number of control points: the same per cent error made on different parameters may have a very different influence on the precision of the calibration output. Therefore a performance index needs to be identified and employed. Standard deviation (SD, see Equation (31)) has already been employed as an index assessing the level of precision reached by the calibration procedure. Following an approach similar to the one described in the two previous phases of the analysis, and holding the assumption that the system behaves linearly, in the fourth phase the effect on SD of a 1%-error on the extrinsic parameter variation estimates is computed. Then, in the fifth phase, these data are combined with those of the third step to yield the influence of acquisition noise on the performance index. Table V, shows the output of the fourth phase, which is the SD measured in μm. Figure 21 represents the output of the fifth phase: it has been obtained multiplying the results of the third and fourth phase, and shows the influence on the performance index of the acquisition noise, plotted with reference to each geometrical parameter and to several different calibration patterns. The imposed parameter variations are reported in the white rectangle. Considering the system linear causes negligible errors also in this phase: through a procedure analogous to the one previously described it has been verified that the absolute per cent error on the values reported in Figure 21 ranges from 0.08% to 1.43%, which does not affect the correctness of the considerations that can be drawn observing the results. A larger number of calibration patterns is reported in Figure 21 than in the previous tables so as to show the data trend better. It can be noticed that the higher the number of control points, the less affected the calibration procedure is by the acquisition

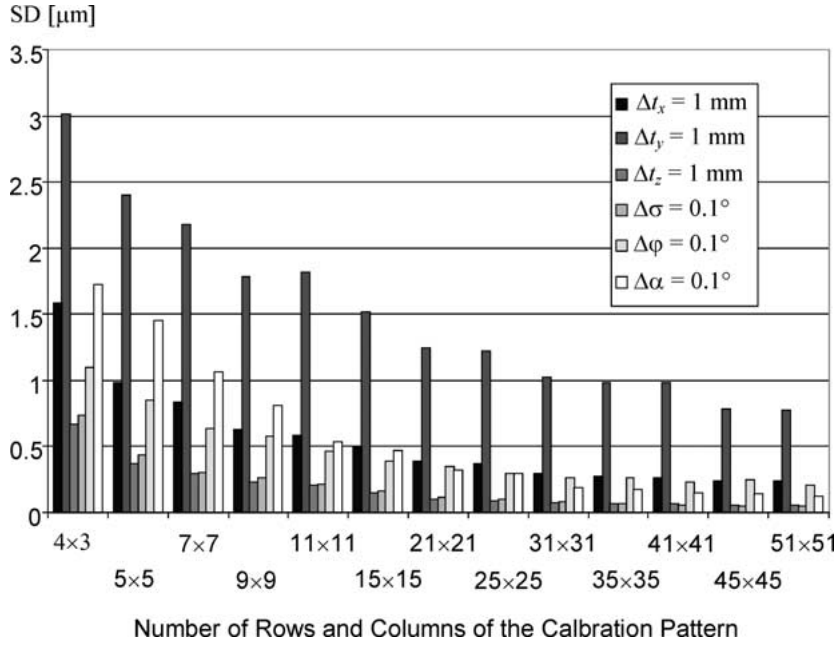

Figure 21. Effect on the performance index of image acquisition noise.

noise and consequently the more precise the estimates of the extrinsic parameters are. Nonetheless, after a steep fall, the performance index decreases gradually, and increasing the number of points does not lead to significant improvements.

The calibration pattern employed is composed of 529 control points arranged in 23 rows and columns. As it can be inferred from Figure 21, the chosen number of control points guarantees a good stability of the procedure to image acquisition noise. The diameter of the circles is 4 mm and the distance among the rows is 14 mm. Such dimensions makes it possible for the camera to clearly view and discriminate also the farthest circles, which appear smaller and closer.

4. Experimental results

Before testing the calibration procedure with real data, numerous simulations have been carried out to tune the gains of the equations, and to verify the capability of the methodology to calibrate the system parameters when random errors are added to the parameter nominal values. Then, adopting the gains and radial distortion coefficients reported in Table VI, the methodology has been applied to the laboratory prototype producing satisfactory results. Figure 22, which shows the overlapped theoretical and distortion-free images of the calibration pattern obtained at the end of the calibration procedure, graphically demonstrates the accuracy of the procedure output. The theoretical or expected image is composed of the gray circles, while the black circles comprises the distortion-free image, obtained compensating

Table VI. Gains of the equations and radial distortion coefficients adopted in the calibration procedure

K_x	K_y	K_z	K_α	K_φ	K_σ	K_1	K_2
2	2.5	1	−0.02	0.1	0.02	0.005	0.0001

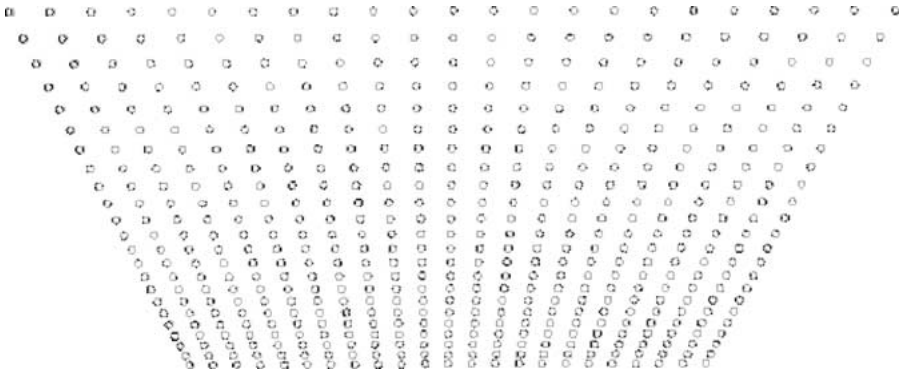

Figure 22. Output of the calibration procedure. The distortion-free (black) and theoretical (gray) images of the calibration pattern are shown overlapped.

the effect of radial distortion and acquisition noise in the image acquired by the camera. When the circles overlap perfectly, only the gray circles are visible in the figure. It can be noticed that at the end of the calibration process a good overlapping of the images is obtained corresponding to a standard deviation of 2.2 μm. Such a subpixel value of the performance index proves the accuracy of the results achieved and confirms the assumption that the intrinsic parameters not calibrated only have a marginal effect on the processed images.

The calibration tables computed updating the mathematical model of the system with the calibrated values of the extrinsic and intrinsic parameters, have allowed scanning objects with a resolution of 0.1 mm and an accuracy of ±0.5 mm.

The time required by the system PC to carry out the calibration procedure, is approximately 90 seconds, including the computation of the elements of the calibration tables. As far as scanning time is concerned, both data acquisition and post-processing take approximately 50 seconds independently of the foot shape and size.

5. Conclusions

Part II of this paper concerns a calibration methodology specifically conceived for the opto-mechanical device presented in Part I. The calibration is performed using the system camera to take a single picture of a planar calibration pattern which is

properly positioned with respect to the laser light planes. The deviations from the nominal values of the extrinsic and intrinsic parameters of the system are computed comparing the theoretical and observed images of the calibration pattern. In particular, it has been possible to establish some interesting relations between the system extrinsic parameters and the main geometrical features of the expected and real images of the control points. The camera intrinsic parameters whose influence on the acquired image is relevant are calibrated through the implemented procedure, while the other intrinsic parameters are assumed to be known in advance.

The chosen calibration pattern is composed of a set of control points whose number has been established on the basis of both geometrical considerations and the results of a statistical analysis investigating the influence of image acquisition noise on the calibration procedure.

The calibration procedure proved to be effective and efficient when tested with the laboratory prototype. In particular, it has been possible to obtain a good value of the performance index defined to assess the accuracy of the output of the calibration procedure.

By introducing the calibrated values of the geometrical and optical parameters into the mathematical model of the system, it has been possible to measure the foot shapes with a satisfactory resolution and accuracy.

In a future work the effect on the system performance, of a different geometry and position of the calibration pattern are being investigated. In particular, the use of a vertical pattern parallel to the light plane, in place of the horizontal pattern, may increase the accuracy of the calibration output, as the points sensed during a foot scan lie on the laser planes, while the currently used control points lie on the footboard plane.

Appendix

The values of the parameters E, F, G and I in Equations (23) and (24) have been computed following the same approach shown in the Appendix of Part I, but considering three points lying on the footboard plane ($z_W = 0$) and not on the light plane. The three points considered have the following homogeneous coordinates:

$$\begin{aligned}
(0, 0, 0, 1)_L^{\mathrm{T}} &\equiv (t_x, t_y, t_z, 1)_C^{\mathrm{T}} \\
(1, 0, 0, 1)_L^{\mathrm{T}} &\equiv (\cos\varphi \sin\alpha + t_x, -\cos\sigma \sin\alpha - \sin\sigma \sin\varphi \cos\alpha + t_y \\
&\quad - \sin\sigma \sin\alpha + \cos\sigma \sin\varphi \cos\alpha + t_z, 1)_C^{\mathrm{T}}, \qquad \text{(A.11)} \\
(0, 0, 1, 1)_L^{\mathrm{T}} &\equiv (-\cos\varphi \sin\alpha + t_x, -\cos\sigma \cos\alpha - \sin\sigma \sin\varphi \sin\alpha + t_y \\
&\quad - \sin\sigma \sin\alpha + \cos\sigma \sin\varphi \sin\alpha + t_z, 1)_C^{\mathrm{T}}.
\end{aligned}$$

The coordinates marked with the subscript L are expressed in the light plane reference while those marked with the subscript C are expressed in the camera reference.

It follows that:

$$\begin{aligned} E &= \sin\varphi, \\ F &= \sin\sigma\cos\varphi, \\ G &= -\cos\sigma\cos\varphi, \\ I &= t_x\sin\varphi + t_y\sin\sigma\cos\varphi - t_z\cos\sigma\cos\varphi. \end{aligned} \tag{A.12}$$

References

Basu, A. and Ravi, K.: 1995, Active camera calibration using pan, tilt and roll, in: *IEEE Internat. Conf. on Robotics and Automation*, pp. 2961–2967.

Batista, J., Araújo, H., and de Almeida, A. T.: 1999, Iterative multistep explicit camera calibration, *IEEE Trans. Robotics Automat.* **15**(5), 897–917.

Beyer, H. A.: 1992, Accurate calibration of CCD-cameras, in: *Proc. of 1992 IEEE Computer Society Conf. on Computer Vision and Pattern Recognition*, pp. 96–101.

Gonzáles, F., Campoy, P., Aracil, R., Peñafiel, F., and Sebastián, J. M: 1993, Three-dimensional digitizer for the footwear industry, *SPIE Comput. Vision Industry* **1989**, 332–338.

Lenz, R. K. and Tsai, R. Y.: 1988, Techniques for calibration of the scale factor and image center for high accuracy 3D machine vision metrology, *IEEE Trans. Pattern Anal. Mach. Intelligence* **10**(5), 713–720.

Martins, H. A., Birk, J. R., and Kelly, R. B.: 1981, Camera models based on data from two calibration planes, *Comput. Graphics Image Process.* **17**, 173–180.

Tsai, R. Y.: 1987, A versatile camera calibration technique for high-accuracy 3D machine vision metrology using Off-the-Shelf TV cameras and lenses, *IEEE J. Robotics Automat.* **3**(4), 323–344.

Wang, L. L. and Tsai, W. H.: 1991, Camera calibration by vanishing lines for 3D computer vision, *IEEE Trans. Pattern Anal. Mach. Intelligence* **13**(4), 370–376.

Wei, G. Q. and De Ma, S.: 1994, Implicit and explicit camera calibration: Theory and experiments, *IEEE Trans. Pattern Anal. Mach. Intelligence* **16**(5), 469–480.

Weng, J., Cohen, P., and Herniou, M.: 1992, Camera calibration with distortion models and accuracy evaluation, *IEEE Trans. Pattern Anal. Mach. Intelligence* **14**(10), 965–980.

Yang, C. and Hu, Z.: 1998, An intrinsic parameters self-calibration technique for active vision system, in: *Proc. of the 14th Internat. IEEE Conf. on Pattern Recognition*, pp. 67–69.

Zhuang, H. and Wu, W. C.: 1996, Camera calibration with a near parallel (ill-conditioned) calibration board configuration, *IEEE Trans. Robotics Automat.* **12**(6), 918–921.